Four-wave mixing and wavelength conversion in quantum dots

David Nielsen* and Shun Lien Chuang†
Department of Electrical and Computer Engineering, University of Illinois at Urbana–Champaign, Urbana, Illinois 61801, USA
(Received 4 August 2009; revised manuscript received 30 October 2009; published 7 January 2010)

We perform a theoretical analysis based on density-matrix equations to determine the nonlinear susceptibilities and gain coefficients for a quantum-dot semiconductor optical amplifier. Our results show that for a single bound-state quantum-dot, carrier relaxation at large current densities is limited by the carrier capture time from the continuum to the bound state. We then compare our results with experiment and show that there is a significant contribution from carrier heating in the four-wave mixing efficiency. Our results and data fit indicate that efficient four-wave mixing on high-speed signals of greater than 160 Gb/s is possible.

DOI: 10.1103/PhysRevB.81.035305 PACS number(s): 78.67.Hc, 78.67.De

I. INTRODUCTION

The future of high-speed, wavelength-division multiplexed networks is dependent on the ability to convert optical signals from one frequency to another to prevent wavelength blocking and reduce the number of frequency channels needed to operate a network. Importantly, it is desirable to achieve this entirely in the optical regime to reduce the number of needed components and thus the cost and device footprint. The three main mechanisms employed for this are cross-gain modulation (XGM), cross-phase modulation (XPM), and four-wave mixing (FWM). For high-speed uses, both XGM and XPM are limited by the carrier lifetime as they are dependent on interband carrier recombination and generation. FWM however, has three different physical mechanisms contributing toward its conversion. The first mechanism is the beating between the pump and probe, which causes carrier-density pulsation (CDP) allowing wave mixing by producing a temporal grating in the device. Like XGM and XPM this mechanism relies on interband processes and is thus limited by the recombination and generation rates of carriers.

However, four-wave mixing also has contributions due to spectral-hole burning (SHB) and carrier heating, which are governed by the much faster carrier-carrier and carrier-phonon-scattering rates allowing for the possibility of converting higher speed signals. Spectral hole burning occurs as the strong pump preferentially depletes resonant carriers while leaving carriers in other energy states unaffected, creating a spectral hole. To return to quasiequilibrium, carriers relax down into the depleted states via carrier-carrier scattering. In quantum wells this can be either intersubband or intrasubband processes and is usually very fast as a result with relaxation times of 10–45 fs.[1,2] However, the carrier localization and discrete density of states in quantum dots (QD) mean that relaxation must occur through either intersubband or interdot processes. The large difference in the density of states between the dots and the wetting layers means that the interdot processes are much slower with carrier capture times from the wetting layer to the dots usually in the few to tens of picoseconds.[3,4] Excited state to ground-state relaxation is much faster due to electron-hole interactions and is typically 100–250 fs.[5–7] These slower relaxation mechanisms in quantum dots allow for deeper spectral holes to form and thus for more efficient wave mixing. While it is true that these slower time constants reduce the overall bandwidth when compared to quantum wells, they are still fast enough to allow efficient conversion of signals in the 100 GHz to THz range.

The last FWM mechanism is carrier heating, in which the temperature of the carriers is raised above that of the lattice and must cool down through carrier-phonon interactions. Carrier heating occurs because stimulated emission from the ground state preferentially removes the lowest energy carriers while free carriers absorb photons increasing their energy state. Both of these effects result in raising the mean energy of the carrier distribution and thus its temperature while the lattice temperature remains unchanged. The hot carrier distribution must then cool down through carrier-phonon collisions. The large carrier density present in quantum wells and bulk can cause carrier heating to be significant due to free-carrier absorption. In quantum dots however, the situation is more complicated. InAs dots grown on GaAs have a large conduction-band offset. This, combined with the discrete energy spectrum reduces the carrier density at which gain is achieved. This in turn reduces the free-carrier absorption and carrier-heating effect. Indeed, previous experimental measurements have shown that carrier heating is negligible.[6] However, in InAs dots grown on InGaAsP, which have a small conduction-band offset, experiments have shown significant carrier heating.[8] Previous theoretical work has focused mostly on spectral-hole burning and is extremely detailed in form and difficult to follow[9] or has relied on a ladder system of rate equations[10] making it difficult to determine the underlying physics and key parameters. In the following sections we will derive a simplified model for four-wave mixing in quantum dots based on a simple single bound state that helps elucidate the physical differences between quantum dots and quantum wells. We will then go on to compare our theory with experiment and discuss the implications of our model.

II. DENSITY-MATRIX THEORY FOR NONLINEAR SUSCEPTIBILITY OF QUANTUM DOTS WITH WETTING LAYERS

Following the method of Uskov *et al.*,[11] we used the density-matrix approach to examine four-wave mixing. To simplify our model, we have examined quantum dots with

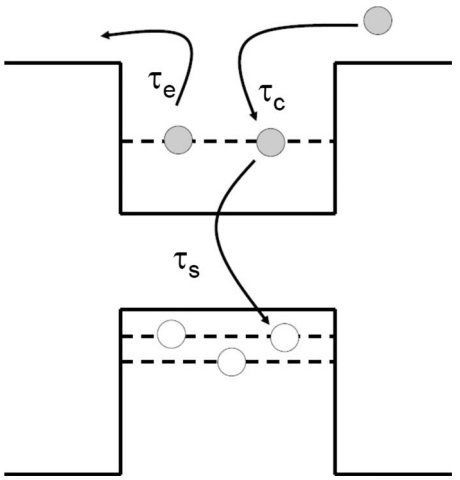

FIG. 1. Diagram of quantum-dot band-structure and carrier-relaxation processes.

only one bound state, taking into account transitions between the bound state and the continuum of the associated wetting layer. Furthermore, as carrier heating relies primarily on carrier-lattice dynamics and not carrier dynamics alone, it is not expected that the results should differ greatly for quantum wells and quantum dots. Thus, we ignore carrier heating in our QD theory and assume quantum-well(QW)-like behavior for carrier heating when we perform our final calculations. A diagram of the theorized carrier dynamics can be seen in Fig. 1. The set of density-matrix equations that describes this system is

$$\dot{\rho}_{cw,k} = \sum_i \frac{\rho_{cd,i}(1-\rho_{cw,k})}{\tau_{i,k}} - \sum_i \frac{\rho_{cw,k}(1-\rho_{cd,i})}{\tau_{k,i}} - \frac{\rho_{cw,k}}{\tau_s} - \frac{\rho_{cw,k} - f_{cw,k}}{\tau_1} + \Lambda_{cw,k}, \tag{1}$$

where ρ is the occupation probability of the state. The subscript cd indicates dot conduction states and the subscript cw indicates wetting-layer conduction states. k indicates the wave vector in the wetting layer and runs over the quantum-well-like states therein, and i runs over every state in the dot ensemble, including each dot twice to account for the spin degeneracy of the states. The first sum is the sum of all carriers escaping from the i dot states into the k wetting-layer state at the rates $\tau_{i,k}$; the second term is the reverse, the total number of carriers lost from the k wetting-layer state into all possible dot states at the rates $\tau_{k,i}$. The third term represents nonradiative recombination, the fourth is spectral-hole burning inside the wetting layer where the occupation probability relaxes back to the Fermi distribution, $f_{cw,k}$, at a rate τ_1 and the final Λ represents carrier injection.

The density-matrix equation for the quantum dots is similarly

$$\dot{\rho}_{cd,i} = -\sum_k \frac{\rho_{cd,i}(1-\rho_{cw,k})}{\tau_{i,k}} + \sum_k \frac{\rho_{cw,k}(1-\rho_{cd,i})}{\tau_{k,i}} - \frac{\rho_{cd,i}}{\tau_s} - \frac{i}{\hbar}(\mu_{vc,i}\rho_{cdvd,i} - \mu_{cv,i}\rho_{vdcd,i})E(t). \tag{2}$$

Here, the last term is the interaction with light, where μ is the transition dipole moment, ρ_{cdvd} is the coherence term of the density-matrix equations, and $E(t)$ is the electric field of the interacting light. Other, higher-order effects such as spontaneous emission and Auger recombination have been ignored in our model.

The governing equation for the coherence terms is simply

$$\dot{\rho}_{cdvd,i} = -(i\omega_i + 1/\tau_2)\rho_{cdvd,i} - \frac{i}{\hbar}\mu_{cdvd,i}(\rho_{cd,i} + \rho_{vd,i} - 1)E(t). \tag{3}$$

Here, decoherence at a rate τ_2 has been included phenomenologically to account for interactions with the outside system. Since the equations for the valence-band states mirror those of the conduction band they need not be typed out and can be determined simply by interchanging the subscripts c and v in Eqs. (1)–(3).

From these density-matrix equations, the general rate equations governing the carrier density in both the dots and wetting layer can be determined by summing over all states and dividing by the volume, V.

$$\frac{1}{V}\sum_k \rho_{cw,k} = N_w, \tag{4}$$

$$\frac{1}{V}\sum_i \rho_{cd,i} = N_d, \tag{5}$$

where N_w represents the carrier density in the continuum and N_d is the carrier density trapped inside the dots.

To integrate over the summations, we assume the time constants are independent of i (all dots release and capture carriers equally) but dependent on k as continuum states closer to the bound state should relax more easily. This allows us to determine normalized expressions for the carrier escape time τ_e and carrier capture time τ_c as $\frac{\tau_e}{C_k} = \frac{\tau_{e,k}}{NV}$ and $\frac{\tau_c}{C_k} = \frac{\tau_{c,k}}{DV}$, respectively. D is the total number of states in the quantum dots, twice the number of quantum dots due to spin degeneracy.

Here the k dependence on the carrier dynamics has been isolated in C_k. The other normalization parameters are D, the density of states in the quantum dots which is equal to twice the dot density due to spin degeneracy, and $N = \frac{1}{V}\Sigma_k C_k$, the effective number of wetting-layer states per volume. There are of course an infinite number of states in the wetting layer if all k states are considered but we expect C_k to fall off with larger k values such that N will be finite. However, we expect it to fall off slowly enough that it will be nearly equal to 1 for wetting-layer states that have significant occupation levels, allowing us to approximate $\frac{1}{V}\Sigma_k C_k \rho_{cw,k} \approx \frac{1}{V}\Sigma_k \rho_{cw,k} = N_w$. By inserting these expressions into the summations we find

$$\frac{1}{V}\sum_k \sum_i \frac{\rho_{cd,i}(1-\rho_{cw,k})}{\tau_{e,k}} = \frac{1}{V}\sum_{k,i} \frac{C_k \rho_{cd,i}(1-\rho_{cw,k})}{NV\tau_e}, \tag{6}$$

$$= \sum_i \frac{\rho_{cd,i}(N - N_w)}{NV\tau_e}, \tag{7}$$

$$= \frac{N_d\left(1-\frac{N_w}{N}\right)}{\tau_e}. \tag{8}$$

Using the same approach the reverse process can be calculated

$$\frac{1}{V}\sum_{k,i}\frac{\rho_{cw,k}(1-\rho_{cd,i})}{\tau_{c,k}} = \frac{N_w\left(1-\frac{N_d}{D}\right)}{\tau_c}. \tag{9}$$

Combining these results with our previous results, we find the following rate equations:

$$\dot{N}_w = \frac{N_d\left(1-\frac{N_w}{N}\right)}{\tau_e} - \frac{N_w\left(1-\frac{N_d}{D}\right)}{\tau_c} - \frac{N_w}{\tau_s} + \frac{I}{qV}, \tag{10}$$

$$\dot{N}_d = -\frac{N_d\left(1-\frac{N_w}{N}\right)}{\tau_e} + \frac{N_w\left(1-\frac{N_d}{D}\right)}{\tau_c} - \frac{N_d}{\tau_s} + 2a(N_d)E(t). \tag{11}$$

Here the sum over the coherence terms has been replaced by

$$a(N_d) = -\frac{i}{\hbar}\frac{1}{2V}\sum_i(\mu_{vc,i}\rho_{cdvd,i} - \mu_{cv,i}\rho_{vdcd,i})E(t) \tag{12}$$

the material absorption of the system (Eq. I.37 of Ref. 12). When normalized and written in terms of the occupation probabilities $f=N_d/D$ and $w=N_w/N$ these equations become the same rate equations which have already been extensively used and studied[10,13–15] validating our starting equations.

$$\dot{w} = \frac{D}{N}\frac{f(1-w)}{\tau_e} - \frac{w(1-f)}{\tau_c} - \frac{w}{\tau_s} + \frac{I}{qVN}, \tag{13}$$

$$\dot{f} = -\frac{f(1-w)}{\tau_e} + \frac{N}{D}\frac{w(1-f)}{\tau_c} - \frac{f}{\tau_s} + 2a_n(f)E(t). \tag{14}$$

Here a_n is the absorption renormalized for the occupation probability f. Importantly, in most circumstances the number of states in the continuum is very large compared to the number of electrons; thus, we can achieve an excellent approximation by taking the limit that $N_w \ll N$ and find that the rate equations become

$$\dot{N}_w = D\frac{f}{\tau_e} - \frac{N_w(1-f)}{\tau_c} - \frac{N_w}{\tau_s} + \frac{I}{qV}, \tag{15}$$

$$\dot{f} = -\frac{f}{\tau_e} + \frac{1}{D}\frac{N_w(1-f)}{\tau_c} - \frac{f}{\tau_s} + 2a'(f)E(t). \tag{16}$$

To calculate the four-wave mixing efficiency, we must determine the susceptibilities. To do this we assume an electric field of the form

$$E(t) = E_0 e^{-i\omega_0 t} + E_1 e^{-i(\omega_0+\delta)t} + E_2 e^{-i(\omega_0-\delta)t} + \text{c.c.}, \tag{17}$$

which is pictured in Fig. 2. Here ω_0 is the pump frequency, δ is the pump-probe detuning, E_0 is the slowly varying amplitude of the pump, E_1 is that of the probe, and E_2 is the conjugate formed through nonlinear mixing. Together these electric fields will create a polarization density of the similar form

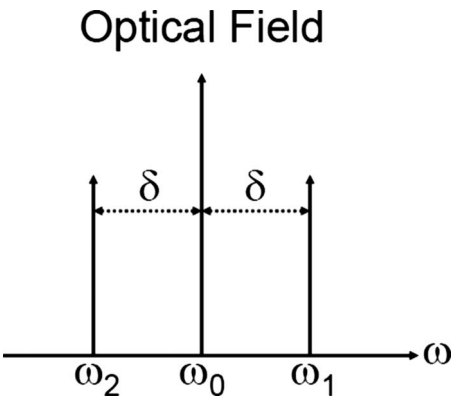

FIG. 2. Diagram of the assumed electric field input with a pump, probe, and conjugate.

$$P(t) = P_0 e^{-i\omega_0 t} + P_1 e^{-i(\omega_0+\delta)t} + P_2 e^{-i(\omega_0-\delta)t} + \text{c.c.} \tag{18}$$

inside the material.

As the polarization density is directly related to the dipole terms

$$P(t) = \frac{1}{V}\sum_{j=i,k}\mu_{vc,j}(\rho_{cv,j} + \rho_{vc,j}) \tag{19}$$

we expect the dipole terms to also follow the same form

$$\rho_{cv,j} = \sigma_{j,0}e^{-i\omega_0 t} + \sigma_{j,1}e^{-i(\omega_0+\delta)t} + \sigma_{j,2}e^{-i(\omega_0-\delta)t}, \tag{20}$$

where j includes both the k continuum states and the discrete i states. As the pump light field is assumed to be on resonance with the quantum dots however and not with the continuum, the contributions from continuum's k states can be ignored.

Due to beating between the pump and probe, we expect both the state occupation probabilities and carrier density to beat in time as

$$\rho_{c,j} = \bar{\rho}_{c,j} + \tilde{\rho}_{c,j}e^{-i\delta t} + \tilde{\rho}^*_{c,j}e^{i\delta t}, \tag{21}$$

$$N_j = \overline{N_j} + \tilde{N}_j e^{-i\delta t} + \tilde{N}^*_j e^{i\delta t}, \tag{22}$$

where j can be replaced by both d and w. As these are incoherent processes, contributions from the continuum and dots must both be considered, unlike the dipole terms where continuum contributions can be ignored. Taking these assumptions and putting them into the density-matrix equations for the quantum-dot states, we can determine the polarizations to first order in E_0

$$P_0 = \frac{1}{V}\sum_{j=i,k}\frac{|\mu_j|^2}{\hbar}\hat{\chi}_j(\omega_0)(\bar{\rho}_{c,j} + \bar{\rho}_{v,j} - 1)E_0, \tag{23}$$

$$P_1 = \frac{1}{V}\sum_{j=i,k}\frac{|\mu_j|^2}{\hbar}\hat{\chi}_j(\omega_1)\times[(\bar{\rho}_{c,j}+\bar{\rho}_{v,j}-1)E_1+(\tilde{\rho}_{c,j}+\tilde{\rho}_{v,j})E_0], \tag{24}$$

$$P_2 = \frac{1}{V}\sum_{j=i,k}\frac{|\mu_j|^2}{\hbar}\hat{\chi}_j(\omega_2)\times[(\bar{\rho}_{c,j}+\bar{\rho}_{v,j}-1)E_2+(\tilde{\rho}^*_{c,j}+\tilde{\rho}^*_{v,j})E_0], \tag{25}$$

where

$$\hat{\chi}_j(\omega) = \frac{1}{\omega-\omega_j+i/\tau_2} \tag{26}$$

is the Lorentzian lineshape determined by the decoherence time and is responsible for homogeneous broadening. To solve these and find the susceptibilities, we must determine $(\bar{\rho}_{cd,i}+\bar{\rho}_{vd,i}-1)$ and $(\tilde{\rho}_{cd,i}+\tilde{\rho}_{vd,i})$ which can be done by performing a steady-state and small-signal analysis of the density matrix and rate equations.

For the steady-state solution, we find

$$(\bar{\rho}_{cd,i}+\bar{\rho}_{vd,i}-1) = \left(\frac{2}{D}\frac{\tau_d}{\tau_c}\bar{N}_w-1\right)-\frac{2i|\mu_i|^2\tau_d}{\hbar^2}(\bar{\rho}_{cd,i}+\bar{\rho}_{vd,i}-1)\times|E_0|^2[\hat{\chi}_i(\omega_0)-\hat{\chi}^*_i(\omega_0)], \tag{27}$$

where

$$\tau_d = \left(\frac{1}{\tau_e}+\frac{1}{D}\frac{\bar{N}_w}{\tau_c}\right)^{-1} \tag{28}$$

and $\bar{N}_w$ is the steady-state solution for N_w from Eqs. (10) and (11) determined by setting $\dot{N}_w=0$. An examination of these equations will show that the steady-state value will be ultimately determined by the injected current and the carrier lifetime including contributions from both nonradiative recombination and stimulated emission. Thus, $\bar{N}_w$ is an external parameter that is controlled via the applied current and pump power. It is important to point out that in Eq. (27) we have assumed that the hole dynamics mirror the electron dynamics in the system.

By comparing our result in Eq. (27) with the results of the same calculations done for bulk,[11] it is clear that τ_d is the equivalent of a spectral-hole burning time constant for quantum dots. Due to charge localization, electrons trapped in quantum dots have no direct interaction with each other and thus cannot redistribute their energy via carrier-carrier interactions to return to thermal equilibrium. Instead, the energy exchange must occur through the continuum with depleted dots capturing new electrons from the continuum and dots which are over populated ejecting electrons to the continuum. τ_d represents the rate at which the quantum-dot ensemble will relax to thermal equilibrium via these capture and escape dynamics. At low wetting-layer carrier densities, the relaxation is limited by how quickly electrons can escape from the overly populated dots; however, as the carrier density in the wetting layer increases, it is the rate of carrier capture that limits the relaxation rate. The above allows us to find a steady-state expression for the occupation probabilities as

$$(\bar{\rho}_{cd,i}+\bar{\rho}_{vd,i}-1) = \frac{\left(\frac{2}{D}\frac{\tau_d}{\tau_c}\bar{N}_w-1\right)}{1+\frac{2i|\mu_i|^2\tau_d}{\hbar^2}|E_0|^2[\hat{\chi}_i(\omega_0)-\hat{\chi}^*_i(\omega_0)]}. \tag{29}$$

When the pump is turned off we expect that the dot occupations probabilities should be the same as the occupation probability under thermal equilibrium, f, such that $(\bar{\rho}_{cd,i}+\bar{\rho}_{vd,i}-1)=(f_{cd}+f_{vd}-1)$. By taking $E_0=0$ in Eq. (29) we find that

$$(f_{cd}+f_{vd}-1) = \left(\frac{2}{D}\frac{\tau_d}{\tau_c}\bar{N}_w-1\right) \tag{30}$$

showing that the occupation probability of the dots is completely dependent on the ratio of τ_d/τ_c and the wetting-layer filling factor. All dots have the same occupation probability under thermal equilibrium because we previously assumed that all dots captured electrons at the same rate. Furthermore, by taking the derivative of Eq. (30) it can be shown that

$$\left(\frac{\partial f_c}{\partial \bar{N}_w}+\frac{\partial f_v}{\partial \bar{N}_w}\right) = \frac{2}{D}\frac{\tau_d}{\tau_c}\left(1-\frac{\tau_d}{\tau_c}\frac{\bar{N}_w}{D}\right). \tag{31}$$

Similar to the steady-state analysis, we perform a small-signal analysis as well and find that to first order in E_0

$$(\tilde{\rho}_{cd,i}+\tilde{\rho}_{vd,i}) = \frac{1}{1-i\delta\tau_d}\left\{\tilde{N}_w\left[(\bar{\rho}_{cd,i}+\bar{\rho}_{vd,i}-1)\left(-\frac{1}{D}\frac{\tau_d}{\tau_c}\right)+\left(\frac{1}{D}\frac{\tau_d}{\tau_c}\right)\right]-\frac{2i\tau_d|\mu_i|^2}{\hbar^2}(\bar{\rho}_{cd,i}+\bar{\rho}_{vd,i}-1)\times\{[\hat{\chi}_i(\omega_1)-\hat{\chi}^*_i(\omega_0)]E^*_0E_1+[\hat{\chi}_i(\omega_0)-\hat{\chi}^*_i(\omega_2)]E_0E^*_2\}\right\}. \tag{32}$$

This result leaves us with the need to determine $\tilde{N}_w$ in order to finalize our solution. For this we return to the rate equations, Eqs. (13) and (14), and perform a small signal analysis to find that

$$\tilde{N}_w = \frac{-X(L_1+L_2)}{WY-XZ}, \tag{33}$$

where

$$L_1 = i\frac{1}{DV}\sum_i\frac{|\mu_i|^2}{\hbar^2}(\bar{\rho}_{cd,i}+\bar{\rho}_{vd,i}-1)\times\{[\hat{\chi}_i(\omega_1)-\hat{\chi}^*_i(\omega_0)]E^*_0E_1+[\hat{\chi}_i(\omega_0)-\hat{\chi}^*_i(\omega_2)]E_0E^*_2\}, \tag{34}$$

$$L_2 = i\frac{1}{DV}\sum_i\frac{|\mu_i|^2}{\hbar^2}(\tilde{\rho}_{cd,i}+\tilde{\rho}_{vd,i})|E_0|^2[\hat{\chi}_i(\omega_1)-\hat{\chi}^*_i(\omega_2)], \tag{35}$$

$$W = \frac{1-\bar{f}}{\tau_c} + \frac{1}{\tau_s} - i\delta, \tag{36}$$

$$X = \frac{D}{\tau_e} + \frac{\bar{N}_w}{\tau_c}, \tag{37}$$

$$Y = \frac{1}{\tau_e} + \frac{1}{D}\frac{\bar{N}_w}{\tau_c} + \frac{1}{\tau_s} - i\delta, \tag{38}$$

$$Z = \frac{1}{D}\frac{1-\bar{f}}{\tau_c}. \tag{39}$$

While this expression may seem complicated, it is fundamentally an expression which takes into account the beating of the light field in L_1, saturation from the pump in L_2 and with a bandwidth determined by the carrier lifetime in the quantum dot which can both escape to or be captured from the wetting layer or recombine nonradiatively. By taking Eq. (32) and substituting it into Eq. (33) we can find an expression for the varying wetting-layer carrier density

$$\tilde{N}_w = \frac{-iX\frac{1}{DV}\sum_i \frac{|\mu_i|^2}{\hbar^2}\left(\frac{2}{D}\frac{\tau_d}{\tau_c}\bar{N}_w - 1\right)\{[\hat{\chi}_i(\omega_1) - \hat{\chi}_i^*(\omega_0)]E_0^*E_1 + [\hat{\chi}_i(\omega_0) - \hat{\chi}_i^*(\omega_2)]E_0E_2^*\}}{WY - XZ + Xi\frac{1}{DV}\sum_i \frac{|\mu_i|^2}{\hbar^2}\left[\left(\frac{2}{D}\frac{\tau_d}{\tau_c}\right)\left(1 - \frac{\tau_d}{\tau_c}\frac{\bar{N}_w}{D}\right)\right]|E_0|^2[\hat{\chi}_i(\omega_1) - \hat{\chi}_i^*(\omega_2)]}, \tag{40}$$

where again we have solved to first order by assuming that

$$(\bar{\rho}_{cd,i} + \bar{\rho}_{vd,i} - 1) = \left(\frac{2}{D}\frac{\tau_d}{\tau_c}\bar{N}_w - 1\right) \tag{41}$$

and

$$(\tilde{\rho}_{cd,i} + \tilde{\rho}_{vd,i}) = \frac{2}{D}\frac{\tau_d}{\tau_c}\left(1 - \frac{\tau_d}{\tau_c}\frac{\bar{N}_w}{D}\right)\tilde{N}_w. \tag{42}$$

Taking these expressions and combining them with our earlier expressions for the polarization densities we find the pump polarization density and linear susceptibility, $\chi^{(l)}$, to be

$$P_0 = \frac{1}{V}\sum_i \frac{|\mu_i|^2}{\hbar}\hat{\chi}_i(\omega_0)\frac{\left(\frac{2}{D}\frac{\tau_d}{\tau_c}\bar{N}_w - 1\right)}{1 + \frac{2i|\mu_i|^2\tau_d}{\hbar^2}|E_0|^2[\hat{\chi}_i(\omega_0) - \hat{\chi}_i^*(\omega_0)]}, \tag{43}$$

$$\chi^{(l)}(\omega) = \frac{1}{\epsilon_0}\frac{1}{V}\sum_i \frac{|\mu_i|^2}{\hbar}\hat{\chi}_i(\omega) \times \frac{\left(\frac{2}{D}\frac{\tau_d}{\tau_c}\bar{N}_w - 1\right)}{1 + \frac{2i|\mu_i|^2\tau_d}{\hbar^2}|E_0|^2[\hat{\chi}_i(\omega_0) - \hat{\chi}_i^*(\omega_0)]}. \tag{44}$$

Similarly, we solve for the probe polarization density

$$\begin{aligned} P_1 = {} & \epsilon_0\chi^{(l)}(\omega_1)E_1 + \frac{1}{V}\sum_i \frac{|\mu_i|^2}{\hbar}\hat{\chi}_i(\omega_1)\left(\frac{1}{1 - i\delta\tau_d}\right) \\ & \times\left[\frac{2}{D}\frac{\tau_d}{\tau_c}\left(1 - \frac{\bar{N}_w}{D}\frac{\tau_d}{\tau_c}\right)\right]\tilde{N}_wE_0 + \frac{1}{V}\sum_i \frac{|\mu_i|^2}{\hbar}\hat{\chi}_i(\omega_1) \\ & \times\left(\frac{1}{1 - i\delta\tau_d}\right)\frac{-2i\tau_d|\mu_i|^2}{\hbar^2}\left(\frac{2}{D}\frac{\tau_d}{\tau_c}\bar{N}_w - 1\right) \\ & \times\{[\hat{\chi}_i(\omega_1) - \hat{\chi}_i^*(\omega_0)]E_0^*E_1 + [\hat{\chi}_i(\omega_0) - \hat{\chi}_i^*(\omega_2)]E_0E_2^*\}E_0. \end{aligned} \tag{45}$$

For P_1 the induced polarization density is split into three terms. The first is the linear polarization density associated with gain or absorption in the optical amplifier. The second terms represent the nonlinear interaction between the pump and probe due to carrier-density pulsation, and the third term is the nonlinear interaction due to spectral-hole burning. The polarization density P_2 is identical to that of P_1 except with the subscripts 1 and 2 interchanged. We seek a way to simplify Eq. (45) so that it can be more easily expressed as

$$\begin{aligned} P_1 = {} & \epsilon_0\chi^{(l)}(\omega_1)E_1 + \epsilon_0\chi^{\mathrm{CDP}}(\omega_1;\omega_0,\omega_1)E_1 \\ & + \epsilon_0\chi^{\mathrm{SHB}}(\omega_1;\omega_0,\omega_1)E_1 + \epsilon_0\chi^{\mathrm{CDP}}(\omega_1;\omega_2,\omega_0)\frac{E_0^2}{|E_0|^2}E_2^* \\ & + \epsilon_0\chi^{\mathrm{SHB}}(\omega_1;\omega_2,\omega_0)\frac{E_0^2}{|E_0|^2}E_2^*, \end{aligned} \tag{46}$$

where the various contributing factors to the susceptibility are separated from each other. These factors include the linear response and the nonlinear responses due to SHB and CDP.

Taking this into account, we can determine generalized susceptibilities due to carrier-density pulsation and spectral-hole burning as

$$\chi^{\mathrm{CDP}}(\omega_1;\omega_2,\omega_3)=\frac{2\epsilon_0(c\eta)^2\dfrac{dg}{dN_w}\tau_s|E_0|^2}{\hbar\omega_0\omega_1}\frac{g(\omega_0)(\alpha+i)}{[1+i(\omega_2-\omega_3)\tau_d]\left[\dfrac{D\tau_s}{X}(WY-XZ)+\dfrac{2\epsilon_0 c\eta\dfrac{dg}{dN_w}\tau_s|E_0|^2}{\hbar\omega_0}\right]}, \tag{47}$$

$$\chi^{\mathrm{SHB}}(\omega_1;\omega_2,\omega_3)=\frac{-2i\tau_d}{\hbar^3}\left[\frac{|E_0|^2}{1+i(\omega_2-\omega_3)\tau_d}\right]\frac{1}{\epsilon_0}\frac{1}{V}\sum_i|\mu_i|^4\hat{\chi}_i(\omega_1)\left(\frac{2}{D}\frac{\tau_d}{\tau_c}\bar{N}_w-1\right)[\hat{\chi}_i(\omega_3)-\hat{\chi}_i^*(\omega_2)], \tag{48}$$

where we have simplified the expression for χ^{CDP} by applying the identities

$$\frac{1}{V}\sum_i\frac{|\mu_i|^2}{\hbar}\hat{\chi}_i(\omega)\frac{2\tau_d}{D\tau_c}\left(1-\frac{\tau_d}{\tau_c}\frac{\bar{N}_w}{D}\right)=-\epsilon_0\frac{c\eta}{\omega}\frac{dg}{dN}(\alpha+i), \tag{49}$$

$$i\tau_s\frac{1}{V}\sum_i\frac{|\mu_i|^2}{\hbar^2}\left(\frac{2}{D}\frac{\tau_d}{\tau_c}\bar{N}_w-1\right)[\hat{\chi}_i(\omega)-\hat{\chi}_i^*(\omega)]=\frac{2c\eta\epsilon_0\tau_s}{\omega\hbar}g(w), \tag{50}$$

which have been derived by taking the similar identities from Ref. 11 and substituting the equivalent values for $(\bar{f}_c+\bar{f}_v-1)$ and $(\frac{\partial f_c}{\partial N}+\frac{\partial f_c}{\partial N})$ in the quantum-dot system identified in Eqs. (30) and (31). These identities also introduce important parameters for comparison to experiment, including the linewidth enhancement factor,[16] α, the refractive index, η, and the material gain, $g(\omega)$, which is calculated from Eq. (44)

$$g(\omega)=-\frac{\omega}{\eta c}\mathrm{Im}[\chi^{(l)}(\omega)]. \tag{51}$$

III. MODEL FOR CONVERSION EFFICIENCY

The theoretical results developed in Sec. II determined the nonlinear susceptibilities χ^{CDP} and χ^{SHB} in addition to the linear susceptibility. For our purpose of examining four-wave mixing, we will use these susceptibilities to calculate the conversion efficiency. For wavelength conversion, efficiency, η_{eff}, is defined as the power out at the new wavelength divided by the power in at the original wavelength, $\eta_{eff}=\frac{|E_2(L)|^2}{|E_1(0)|^2}$. To calculate this efficiency, we use the analytical solution developed by Ref. 17 to determine the output power at the conjugate wavelength. The analytical solution for the output intensity of the light fields after propagating through a device of length L is

$$E_0(L)=e^{\bar{G}/2(1-i\alpha)}\left[1+F_-(L,\delta)\frac{|E_1(0)|^2}{E_{sat}^2}\right]E_0(0), \tag{52}$$

$$E_1(L)=e^{\bar{G}/2(1-i\alpha)}\left[1+F_+(L,\delta)\frac{|E_0(0)|^2}{E_{sat}^2}\right]E_1(0), \tag{53}$$

$$E_2(L)=e^{\bar{G}/2(1-i\alpha)}F_-(L,\delta)\frac{E_0(0)^2}{E_{sat}^2}E_1^*(0), \tag{54}$$

$$F_\pm(L,\delta)=-C\frac{e^{\bar{G}}-1}{2}\left[\frac{1-i\alpha}{1+\dfrac{|E_0(0)|^2}{E_{sat}^2}\pm i\delta\tau}+\sum_x\frac{\kappa_x(1-i\alpha_x)}{1\pm i\delta\tau}\right]. \tag{55}$$

In these equations, $\bar{G}$ is the steady-state, integrated device gain defined as the steady-state solution to

$$\frac{dG}{dt}=\frac{G_0-G}{\tau}-(e^G-1)\frac{|E(0)|^2}{\tau}, \tag{56}$$

where τ is the gain recovery time. G is the integrated device gain

$$G=\int_0^L\Gamma g(z,t)dz \tag{57}$$

and G_0 is the unsaturated, integrated gain. C is a phenomenological parameter used to compensate for the nonplane-wave nature of the waveguide modes[17] and has been taken to be 0.8. In Eq. (57) $g(z,t)$ is the material gain and is multiplied by the confinement factor of the waveguide, Γ to account for the fact that the entire light field does not overlap with active media. Since in four-wave mixing the dominant light field is the pump, we took the gain at the pump wavelength when determining $\bar{G}$.

In Eq. (55), the terms in brackets represent the nonlinear interactions with the first being CDP and the sum over x representing all other nonlinear interactions, such as spectral-hole burning and carrier heating whose strengths are determined by the normalized nonlinear gain coefficients κ_x. Combining Eqs. (52)–(54) the FWM efficiency becomes easy to derive as

$$\eta_{eff}=e^{\bar{G}}|F_-(L,\delta)|^2\left[\frac{E_0(0)^2}{E_{sat}^2}\right]^2. \tag{58}$$

While originally derived for a simple quantum-well model, the above, Eqs. (52)–(55), can be adapted to our rigorous quantum-dot model. To begin this adaptation we first define the saturation field for the QD system as

$$E_{sat}^2 = \frac{\hbar\omega_0}{2\epsilon_0 c\,\eta\frac{dg}{dN}\tau_s}. \tag{59}$$

Similarly, the CDP term of $F_{\pm}$ must be rewritten to account for the more complicated dynamics. This is done by comparing the above expression with the solution for the quantum-well susceptibilities calculated in Ref. 11 and our derived quantum-dot susceptibilities. From this comparison we find

$$F_{\pm}^{\mathrm{QD}}(L) = -C\frac{e^{\bar{G}}-1}{2}\left[\frac{1-i\alpha}{\frac{D\tau_s}{X}(WY-XZ)+\frac{|E_0(0)|^2}{E_{sat}^2}} + \sum_x \frac{\kappa_x(1-i\alpha_x)}{1\pm i\delta\tau}\right]. \tag{60}$$

An examination of Eq. (55) will show that the CDP nonlinear gain coefficient is of the same form as the CDP susceptibility except that the numerator is $1-i\alpha$ so that $\kappa_{\mathrm{CDP}}=1$. From this observation, we can determine the nonlinear gain coefficient for spectral-hole burning by normalizing the SHB susceptibility to the CDP susceptibility. The result of this normalization is

$$\kappa_{\mathrm{SHB}}(1-i\alpha_{\mathrm{SHB}}) = \frac{i2\tau_d\omega_0}{c\,\eta\epsilon_0\tau_s\frac{dg}{dN}} \times \left[\frac{\Sigma_k\frac{|\mu_k|^4}{\hbar^2}\hat{\chi}_k(\omega)\left(\frac{2}{D}\frac{\tau_d}{\tau_c}\bar{N}_w-1\right)[\hat{\chi}_k(\omega_0)-\hat{\chi}_k^*(\omega)]}{\sum_k\frac{|\mu_k|^2}{\hbar}\left(\frac{2}{D}\frac{\tau_d}{\tau_c}\bar{N}_w-1\right)[\hat{\chi}_k(\omega)-\hat{\chi}_k^*(\omega)]}\right]. \tag{61}$$

Carrier heating was included in our calculation by relying on the same formulation for the nonlinear susceptibility as is found in quantum wells and bulk. As shallow quantum dots have the majority of their free carriers in the wetting and barrier layer this is considered a good approximation of the actual underlying physics. Keeping with the expression for χ^{CH} found in Ref. 11 and normalizing as we did to find χ^{SHB} we find that

$$\kappa_{CH} = \frac{\tau_{ch}}{\tau_s}\frac{\partial g/\partial T}{\partial g/\partial N}\frac{\Delta E}{h_c}\left[1+\frac{\sigma N}{g(\omega)}\frac{\hbar\omega_0}{\Delta E}\right]. \tag{62}$$

Here ΔE is the energy difference between the chemical potential, the energy needed to add one electron to the continuum, and the energy of an electron in a quantum-dot bound state. τ_{CH} is the rate at which the electron gas cools back to the lattice temperature. h_c is the heat capacity of the free electrons assuming a two-dimensional (2D) electron-gas model

$$h_c = \frac{\pi}{3}\frac{k_b^2 T}{\hbar^2}\frac{m^*}{l}, \tag{63}$$

where m^* is as usual the effective mass for the electrons or holes and l is the effective height of the quantum-dot layer. For our calculations, it was considered to be the distance between adjacent quantum-dot layers, which for our sample was 10 nm. The free-carrier-absorption cross section, σ, was calculated from the Drude model to be

$$\sigma = \frac{q^3\lambda^2}{4\pi^2\epsilon_0 n m^{*2}\mu} \tag{64}$$

but was found to be too small to have an impact on carrier heating due to the low carrier concentration at which gain can be achieved in quantum dots. Instead the primary carrier-heating mechanism is not free-carrier absorption but instead the gain of the device removing the lowest energy carries from the dots while higher-energy electrons are injected into the sample. The ratio $\frac{\partial g}{\partial T}/\frac{\partial g}{\partial N}$ can be found analytically for the quantum-dot system by observing that $g\propto(f_c+f_v-1)$ and that under large bias the majority of carriers actually reside in the barrier and wetting layers. Under these conditions the derivatives can be easily taken giving an analytical solution of

$$\frac{\partial g}{\partial T}/\frac{\partial g}{\partial N} = \frac{-N_w\Delta E}{k_b T^2}. \tag{65}$$

This, when combined with the assumption that carrier heating from free-carrier absorption is insignificant, results in the expression

$$\kappa_{CH} = \frac{3\tau_{ch}N\Delta E^2\hbar^2 L}{\pi\tau_s(k_b T)^3 m^* h_c}. \tag{66}$$

This allows for an analytical calculation of the nonlinear gain coefficient due to carrier heating in quantum dots. Changes in temperature also have a line-width enhancement factor associated with them as the varying occupation probabilities change both the real and imaginary parts of the susceptibility. In a quantum dot we expect the line-width enhancement factor due to temperature changes, α_{CH}, to be very close to the line-width enhancement factor due to carrier-density changes, α, as the raising and lowering of the carrier temperature serves only to change the ratio between the dot and wetting-layer occupation probabilities and thus the number of carriers in the dots. Therefore, these values were set equal to each other.

IV. NUMERICAL RESULTS

For theoretical calculations to have merit, it is important that they can be easily compared and matched with experiment. For this we have performed a simple four-wave mixing experiment in a semiconductor optical amplifier composed of seven layers of InAs QDs grown on InGaAsP which was lattice matched to InP. The total device length was 2 mm.

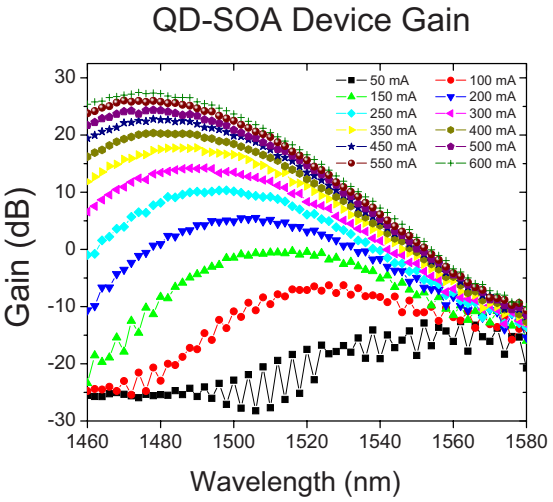

FIG. 3. (Color online) Gain of the QD-SOA for various bias currents.

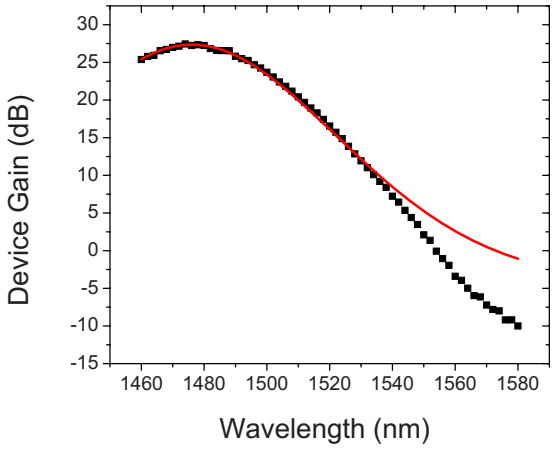

FIG. 4. (Color online) Fit of gain data at 600 mA bias current showing good agreement at the experimental wavelengths of 1490 nm. Deviation at low wavelength is most likely due to free-carrier absorption which was not included in the fitting model.

Importantly, gain and photoluminescence measurements showed no excited state in these dots allowing for a direct comparison to our derived model.

Figure 3 shows the gain spectra of the device at various bias currents. As can be seen in the plot, increasing the bias current has two effects. First, the peak gain increases, and second, the peak wavelength shifts toward shorter wavelengths. This blueshifting of the peak shows that not all dots fill at the same rate. Rather, lower energy dots fill first. Furthermore, this blueshifting will result in a large line-width enhancement factor. Measurements on a similar quantum-dot sample fabricated into a Fabry-Perot laser measured a line-width enhancement factor of 5. For comparison to experiment we thus used $\alpha=\alpha_{CH}=5$. While this value is large for quantum dots, theoretical results have shown that shallow QDs, such as those used, will have larger line-width enhancement factors due to increased coupling between the bound state and barrier layer.[18] While the shifting gain peak at low bias goes against one of our initial assumptions, that all dots fill at the same rate, at high bias we can see the shift is greatly diminished. This is because at large bias current the high dot occupation probability causes the energy difference between the dots to become a minor factor in the carrier dynamics. This results in all dots filling at nearly the same rate as assumed in our model.

To perform four-wave mixing measurements, we sent both a strong pump and a weaker tunable probe into the QD sample. Though the gain peaks at 1480 nm, the limitations of our tunable lasers required that the pump laser be placed slightly off of the gain peak at 1490 nm so that we could scan both positive and negative pump-probe detunings. The tunable probe laser was then swept across the pump and the output spectrum measured on an optical spectrum analyzer (OSA). The amplified spontaneous emission was then subtracted and the efficiency calculated by comparing the power of the output conjugate to the input probe. Due to the resolution limitations of our OSA, detunings of less than 150 GHz could not be measured as the strong pump would wash out the weaker conjugate signals.

To fit these experimental conditions to theory, we first fit the gain spectra of the device using a simple Gaussian approximation for the distribution of dot sizes. To do this we assumed that

$$\Gamma g(\omega) = \Gamma g_0 e^{-(\hbar\omega - \hbar\omega_0)^2/2\sigma^2} - \alpha_i. \tag{67}$$

Here ω_0 is the peak-gain wavelength of 1480 nm. α_i is the intrinsic loss assumed to be 5 cm^{-1}. σ and Γg_0 were fitting parameters representing the width of the dot distribution due to inhomogeneous broadening and the maximum modal gain of the sample, respectively. The best fit can be seen in Fig. 4, where σ was found to be 26 meV and Γg_0 was 36.50 cm^{-1}. While the fit shows excellent agreement near the gain peak, the absorption of long-wavelength light is much higher than expected from this simple model. Attempts were made to correctly match the entire curve by increasing the intrinsic loss but this resulted in unphysically high values. This extra loss is most likely due to a deviation in the inhomogeneous broadening from a Gaussian profile. As our data was taken near the peak wavelength and our theory is based on an assumption of operating near the peak wavelength as well, this variation from the theoretical model was not considered significant for the results presented here.

Once the gain was fit, the gain of the QD Device, along with κ_{SHB}, τ_d and the dot occupation probability, f, were calculated using Eqs. (28), (30), (44), and (61). To perform the summation over all states necessary for calculating κ_{SHB}, the material gain, and the quasi-Fermi levels in the wetting layer, we integrated over the density of states, $\rho(\varepsilon)$. This was assumed to have the form

$$\rho(\epsilon) = \begin{cases} \dfrac{D}{\sqrt{2\pi\sigma^2}} e^{-(\varepsilon - E_b)^2/2\sigma^2} & \varepsilon < E_b + \Delta E \\ \dfrac{m^*}{\pi\hbar^2 l} & \varepsilon > E_b + \Delta E \end{cases}. \tag{68}$$

This includes a single, inhomogeneously broadened bound state in the quantum dots, and a 2D-like continuum of states in the barrier layer. m^* is the effective mass of the electrons

and E_b represents the mean bound-state energy in the dots and is equal to $\hbar\omega_0$.

Utilizing this density of states, calculations were performed at several current densities by recalculating the quasi-Fermi level for each desired current density and then calculating the desired parameters. Other physical parameters necessary for the calculations had to be determined as well. The differential gain, $\frac{dg}{dn}$, was determined from Fig. 3 to be 6.0×10^{-16} cm^2. The carrier-capture time was assumed to be 1 ps in agreement with previous experiments[4] and the escape time was related through the Boltzman factor such that $\tau_e = \tau_c e^{-\Delta E/kT}$ and ΔE was assumed as 0.075 eV, a typical value for quantum dots. The device temperature corresponded to our experimental condition of 288 K. The total number of states in the dots $D=2\times10^{17}$ cm^{-3} was determined from the area dot density of 10^{11} cm^{-2} per dot layer with each layer being 10-nm thick. The factor of 2 is, as stated before, from spin degeneracy. $|\mu(\omega)|^2$ was calculated by equating the gain model of Ref. 12 with that of Ref. 11 to find that

$$|\mu(\omega)|^2 = \frac{e^2}{m_0^2\omega^2}|\hat{e}\cdot p_{cv}|^2. \tag{69}$$

For bulk, the momentum matrix element is known $|\hat{e}\cdot p_{cv}|^2_{bulk}=\frac{m_0}{6}E_p$. For quantum dots, we expect the result to be the same as a quantum well as self-assembled quantum dots are much wider than they are tall. For TE-polarized light we thus expect that $|\hat{e}\cdot p_{cv}|^2_{dot}=\frac{3}{2}|\hat{e}\cdot p_{cv}|^2_{bulk}$ for the conduction subband to the top heavy-hole subband transition and find that

$$|\mu(\omega)|^2 = \frac{e^2E_p}{4m_0\omega^2}, \tag{70}$$

where E_p is the optical matrix parameter and for InAs dots is 22.2 eV,[12] and m_0 is the free electron mass.

The results of these calculations can be seen in Fig. 5 where instead of material gain, the integrated, modal gain $G_0(\omega_0)=\Gamma g_0 L$ has been plotted. These calculations show two expected trends. First, increasing the carrier density causes the dot occupation probability to increase from 0 to 1 with the integrated gain increasing proportionally. Second, κ_{SHB} is proportional to τ_d and decreases with increasing carrier density. This is significant for two reasons. First, the proportionality between κ_{SHB} and τ_d shows those slower carrier relaxation times allow for more efficient four-wave mixing providing a trade off between bandwidth and efficiency. Higher efficiency results in lower bandwidth while large bandwidth reduces efficiency. This is also the fundamental reason that quantum dots should be more efficient for telecommunications applications than quantum wells at speeds in between 10–160 GHz. These speeds are slow enough that the 0.1–1 ps relaxation time of quantum dots can easily convert them. The faster, 50–10 fs,[1,2] relaxation times present in quantum wells result in less efficient conversion but with a much larger bandwidth.

Furthermore, the decrease in κ_{SHB} with increasing bias is not unexpected. κ_{SHB} is a measure of the creation rate of conjugate photons and they are created through the simultaneous absorption of two pump photons and stimulated emission of a probe and conjugate photon. For this to occur there must be unoccupied dots capable of absorbing pump photons. While this at first might cause the belief that the conversion is most efficient at low bias where the dot occupation is low, it is important to remember that the gain and absorption of the sample plays a large role as well. Once a conjugate beam is started, the gain of the sample will amplify it allowing a small conjugate to quickly grow. As the gain reaches a maximum and plateaus after all dots are filled, the nonlinear gain-coefficient plateaus as well resulting in an optimal carrier density. This effect can be seen in Fig. 6 where the efficiency is plotted vs carrier density showing a clear

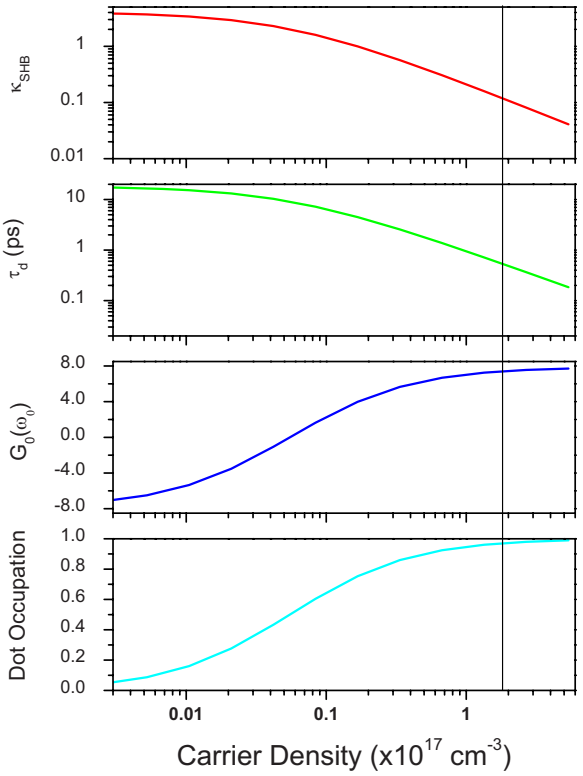

FIG. 5. (Color online) κ_{SHB}, τ_d, $h_0(\omega_0)$, and the dot occupation probability plotted as a function of carrier density. Solid vertical line is the fitting condition.

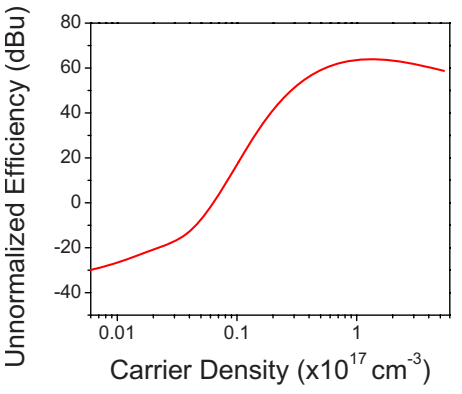

FIG. 6. (Color online) Unnormalized efficiency vs carrier density. Plot does not take into account carrier saturation or pump power so absolute values should not be considered correct.

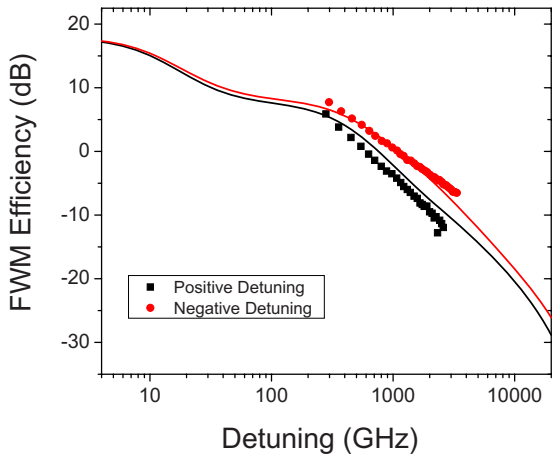

FIG. 7. (Color online) Experimental data with fit. Experiment is shown as points while matching theory is solid lines.

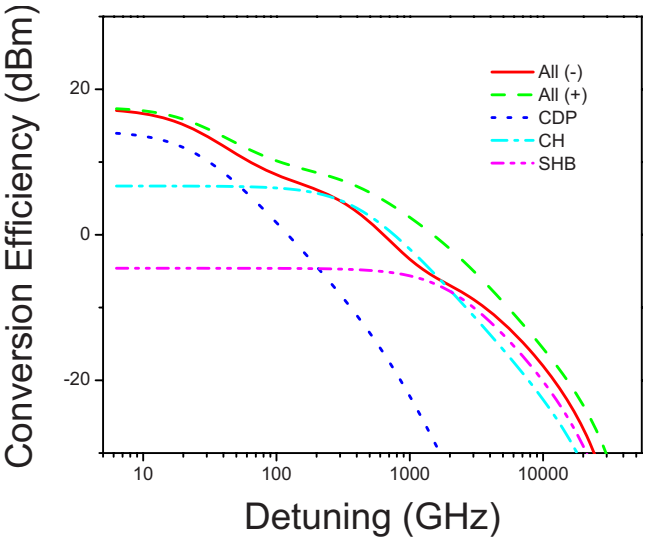

FIG. 8. (Color online) Theoretical efficiency plots with individual contributions from carrier-density pulsation, carrier heating, and spectral-hole burning superimposed. All(−) indicates negative detuning while All(+) indicates positive detuning.

peaking. It is important to point out that for comparison purposes gain saturation and pump power have not been considered in this plot. P/P_{sat} was simply taken to be 1 for the calculation of E_2 but no saturation effects were applied to the gain. In general saturation can play a large role in the ideal pump power.[17] This shows that for true optimization both pump power and carrier density must be considered.

To compare our four-wave mixing data to theory, we took the previous gain fit and calculated the integrated gain over the 2-mm-long device and compared it to the calculated integrated gain. With no good measurement of the confinement factor, it was allowed to drift over typical values for a quantum-dot SOA with the best fit resulting in $\Gamma=2.7\%$ for an integrated gain of 7.3. While this confinement factor is small, this is in the range for a typical quantum-dot device. The vertical line in Fig. 5 shows the carrier density, which provides the best fit and is in agreement with our previous gain fit. It shows calculated values for $\tau_d=0.5$ ps, $\kappa_{\mathrm{SHB}}=0.11$ with $\alpha_{\mathrm{SHB}}=0.013$ being found from the phase of κ_{SHB} while α_{SHB} was included in our calculations, the small magnitude resulted in it having no real effect on the outcome. The carrier-heating effect included contributions from both holes and electrons for a total $\kappa_{CH}=0.08$. This is larger than for typical quantum well and bulk structures due to the slower thermal relaxation measured by Ref. 8.

Other important theoretical parameters were assumed including $\tau_s=200$ ps, an assumed value typical of semiconductor devices under large bias. $\tau_{CH}=2.5$ ps in agreement with experimental measurements in similar quantum dots.[8] The input pump value was chosen to match experiment at $0.16P_{sat}$.

A comparison between our theoretical model and our experimental measurements can be seen in Fig. 7. The fit shows generally good agreement between theory and experiment, both in the magnitude of the conversion efficiency, and in the splitting between positive and negative detunings.

V. DISCUSSION

The efficiency plot from our theory shows two plateaus. One with a bandwidth of a few GHz due to carrier density pulsation and another that extends out to around 200 GHz before falling off. By utilizing the detuning range that lies on the second plateau it is possible to perform high-efficiency wavelength conversion at high-speed frequencies greater than 160 Gb/s by utilizing the four-wave mixing effect. Calculations on typical quantum wells put the efficiency much lower[17] along with previous experimental measurements directly comparing quantum dots and quantum wells.[19]

Importantly, the second plateau is determined more by carrier heating than by spectral-hole burning. This becomes readily apparent when the individual contributions to four-wave mixing are plotted in Fig. 8. While at first one might expect spectral-hole burning to have a large contribution as $\kappa_{\mathrm{SHB}}>\kappa_{CH}$, the large temperature line-width enhancement factor increases the contribution from carrier heating above that of spectral-hole burning. This result demonstrates that in shallow dots with a single bound state the primary four-wave mixing mechanism at large detunings and for high-speed signals is carrier heating. This is in contrast to most other theories which focus mainly on spectral-hole burning[9,10] in quantum dots. This large contribution from carrier heating is possible due to the very slow thermal relaxation rate that occurs in these dots.

This slow relaxation is most likely due to the slow means by which carriers in the wetting layer can relax down into the quantum dots, which have been depleted through stimulated emission. Indeed the measured thermal relaxation time of 2.5 ps is similar to the carrier capture time of 1 ps. As a result we expect deep quantum dots with large energy offsets between the barrier layer and bound state to perform less efficiently as they have a reservoir of excited states which can quickly relax down and buffer the slow carrier capture. The drawback being that these shallow quantum dots, while being more efficient, cannot achieve the same symmetric conversion that has been reported in deeper quantum dots[20] due to their larger line-width enhancement factor caused by cou-

pling to the continuum states. As both spectral-hole burning and carrier heating are seen to be heavily reliant on a slow carrier-capture time for high efficiency, this factor becomes our limiting value in determining the maximum four-wave mixing efficiency and bandwidth in shallow quantum dots.

VI. CONCLUSION

We have developed a theoretical model for four-wave mixing in quantum dots based on density-matrix theory. Using this theory we have calculated the nonlinear gain coefficients due to spectral-hole burning and applied an analytical solution to find the total conversion efficiency. Our model gives excellent quantitative and qualitative agreement with experiment, and demonstrates that the unique carrier dynamics of quantum dots should allow for efficient wavelength conversion of high-speed signals near 160 Gb/s using four-wave mixing.

ACKNOWLEDGMENTS

This work at the University of Illinois was supported by the Defense Advanced Research Project Agency (DARPA) under the University Photonic Center Program (CONSRT). The authors would also like to acknowledge Donghan Lee of Chungnam National University in Daejeon, Korea for his collaboration in providing the quantum-dot device whose gain measurements were used for fitting parameters (Ref. 19).

*Also at the Department of Physics; dcnielse@illinois.edu
†s-chuang@illinois.edu

[1] R. A. Kaindl, S. Lutgen, M. Woerner, T. Elsaesser, B. Nottelmann, V. M. Axt, T. Kuhn, A. Hase, and H. Künzel, Phys. Rev. Lett. **80**, 3575 (1998).
[2] W. H. Knox, D. S. Chemla, G. Livescu, J. E. Cunningham, and J. E. Henry, Phys. Rev. Lett. **61**, 1290 (1988).
[3] D. G. Deppe and H. Huang, IEEE J. Quantum Electron. **42**, 324 (2006).
[4] J. Urayama, T. B. Norris, H. Jiang, J. Singh, and P. Bhattacharya, Appl. Phys. Lett. **80**, 2162 (2002).
[5] P. Borri, W. Langbein, J. Mørk, J. M. Hvam, F. Heinrichsdorff, M.-H. Mao, and D. Bimberg, Phys. Rev. B **60**, 7784 (1999).
[6] P. Borri, W. Langbein, J. Hvam, F. Heinrichsdorff, M.-H. Mao, and D. Bimberg, IEEE J. Sel. Top. Quantum Electron. **6**, 544 (2000).
[7] J. Urayama, T. B. Norris, J. Singh, and P. Bhattacharya, Phys. Rev. Lett. **86**, 4930 (2001).
[8] A. J. Zilkie, J. Meier, P. W. E. Smith, M. Mojahedi, J. S. Aitchison, P. J. Poole, C. N. Allen, P. Barrios, and D. Poitras, Proc. SPIE **5971**, 59710G (2005).
[9] M. Sugawara, H. Ebe, N. Hatori, M. Ishida, Y. Arakawa, T. Akiyama, K. Otsubo, and Y. Nakata, Phys. Rev. B **69**, 235332 (2004).
[10] O. Qasaimeh, IEEE Photon. Technol. Lett. **16**, 993 (2004).
[11] A. Uskov, J. Mork, and J. Mark, IEEE J. Quantum Electron. **30**, 1769 (1994).
[12] S. L. Chuang, *Physics of Optoelectronic Devices* (John-Wiley & Sons, New York, 1995).
[13] J. Kim, H. Su, S. Minin, and S. L. Chuang, IEEE Photon. Technol. Lett. **18**, 1022 (2006).
[14] T. W. Berg, S. Bischoff, I. Magnusdottir, and J. Mork, IEEE Photon. Technol. Lett. **13**, 541 (2001).
[15] M. Sugawara, T. Akiyama, N. Hatori, Y. Nakata, H. Ebe, and H. Ishikawa, Meas. Sci. Technol. **13**, 1683 (2002).
[16] C. H. Henry, IEEE J. Quantum Electron. **18**, 259 (1982).
[17] M. Shtaif and G. Eisenstein, Appl. Phys. Lett. **66**, 1458 (1995).
[18] J. M. Vazquez, H. H. Nilsson, J.-Z. Zhang, and I. Galbraith, IEEE J. Quantum Electron. **42**, 986 (2006).
[19] D. Nielsen, S. L. Chuang, N. J. Kim, D. Lee, S. H. Pyun, W. G. Jeong, C. Y. Chen, and T. S. Lay, Appl. Phys. Lett. **92**, 211101 (2008).
[20] T. Akiyama, H. Kuwatsuka, N. Hatori, Y. Nakata, H. Ebe, and M. Sugawara, IEEE Photon. Technol. Lett. **14**, 1139 (2002).